Bulletin of the JSME

Vol.X, No.X, XXXX

Heat transfer enhancement and torque reduction by traveling wave-like blowing and suction in turbulent Taylor–Couette flow

Hiroya MAMORI*, Koji FUKUDOME**, Kohei OGINO**, Naoya FUKUSHIMA*** and Makoto YAMAMOTO**

* Department of Mechanical and Intelligent Systems Engineering, Faculty of Informatics and Engineering, The University of Electro-Communications
1-5-1 Chofugaoka, Chofu, Tokyo, 182-8585, Japan
E-mail: mamori@uec.ac.jp

** Department of Mechanical Engineering, Faculty of Engineering, Tokyo University of Science
6-3-1, Niijuku, Katsushika, Tokyo, 125-8585, Japan

*** Department of Prime Mover Engineering, Faculty of Engineering, Tokai University
4-1-1, Kitakaname, Hiratsuka, Kanagawa, 259-1292, Japan

Received 22 May 2020

Abstract

Direct numerical simulations of turbulent Taylor–Couette flows are performed to investigate the effect of a traveling wave control on torque and heat transfer. In the Taylor–Couette flow, inner and outer cylinders are rotating and immobile, respectively, and the temperature difference between cylinder walls is maintained as constant. The ratio between the inner and outer cylinder is 0.882, and the Reynolds number is set as 84,000. A traveling wave-like blowing and suction is imposed on an inner cylinder wall. A parametric study shows the effect of control parameters on torque and heat transfer. We focused on three characteristic parameter sets: heat transfer enhancement, relaminarization phenomenon, and simultaneous achievement of torque reduction and heat transfer enhancement. We employed identity equations by using three-component decomposition to clarify contributions from advection, turbulence, and diffusion on torque and Stanton number. The results indicated that the traveling wave control affects the turbulence and advection contributions.

Key words : Direct numerical simulation, Taylor–Couette turbulent flow, traveling wave control, torque reduction, heat transfer

1. Introduction

Heat transfer enhancement is an extremely important contributor e.g., in heat exchangers. When the turbulence is promoted by flow control techniques, turbulent vortical structures are activated and heat transfer is enhanced. However, the skin-friction drag significantly increases and it also results in energy loss. This is due to an analogy between the momentum and heat transfer: similarity in the wall value (i.e., the friction drag and wall heat flux), boundary conditions, and governing equations (i.e., Navier-Stokes and energy equations). They are well-known as Reynolds or Colburn analogies (Reynolds, 1901; Chilton and Colburn, 1934). The identity equations of the skin-friction coefficient C_f and Stanton number St in channel flows (Fukagata et al., 2002; Kasagi et al., 2012) also imply a similarity. The equations are

$$C_f = \frac{12}{\mathrm{Re}} + 12\int_0^1 2(1-y)(-\overline{u'v'})dy, \quad \mathrm{St} = \frac{2}{\mathrm{RePr}} + \int_0^1 \left(-\overline{v'T'}\right)dy. \tag{1}$$

Here, Re is a Reynolds number based on the bulk velocity and channel half height and Pr is a Prandtl number. The first and second terms are contributions from the laminar and turbulent flow, respectively. The contribution

from the turbulence denotes the integration of the Reynolds shear stress ($-\overline{u'v'}$) and turbulent heat flux ($-\overline{v'T'}$), and they are related to the activity of the vortical structures. We note that Eq. (1) is obtained from the no-slip conditions for velocities and the constant temperature difference condition for the temperature. The similarity between identity equations further increases the difficulty of simultaneously enhancing heat transfer and reducing skin-friction drag. Recent studies reported that the effective heat transfer state is obtained by a large-scale intermittent flow structure in the transitional-regime flow when compared to the uniform turbulence beyond the transitional region by using the dissimilarity analysis (Fukudome et al., 2019). However, simultaneous achievement of heat transfer enhancement and skin-friction drag reduction is generally difficult in a fully developed turbulent flow.

The present study employs traveling wave control to obtain dissimilar control effects between skin-friction (or torque) reduction and heat transfer enhancement. The traveling wave-like blowing and suction was initially investigated by Min et al.(2006). They mainly focused on the skin-friction drag reduction effect, i.e., the skin-friction drag is maintained below that of the turbulent flow in the fully developed turbulent channel flow. Subsequently, the mechanism of the skin-friction drag in laminar flow is discussed based on linear analysis (Mamori et al., 2010). The traveling wave stabilizes flows (Lee et al., 2008), controls the onset of the transition (Moarref and Jovanović, 2010; Lieu et al., 2010), and induces the relaminarization phenomenon (Nakanishi et al., 2012; Mamori et al., 2014; Koganezawa et al., 2019). Recently, Nabae et al.(2020) investigated the effect of Reynolds number on skin-friction drag reduction by the traveling wave-like wall deformation and proposed a semi-empirical formula to predict for the drag reduction rate at practically high Reynolds numbers. Additionally, the control includes another attractive effect that denotes the dissimilar control effect of the skin-friction drag reduction and heat transfer enhancement. Higashi et al.(2011) performed a laminar analysis to show the possibility of simultaneous control of skin-friction drag reduction and heat transfer augmentation by traveling wave-like blowing and suction in laminar channel flow. They also performed direct numerical simulations (referred as DNS, hereafter) to confirm the dissimilar control effect in a fully developed turbulent channel flow. Uchino et al.(2017) discussed a DNS to investigate the dissimilar effect by the traveling wave-like wall-deformation instead of blowing and suction. Recently, Kaithakkal et al.(2020) performed a parametric study by DNS to study optimal control parameter sets of the traveling wave-like blowing and suction for the dissimilar control effect in a fully developed turbulent channel flow. The mechanism is discussed based on the unsteady Reynolds averaged Navier-Stokes approach. In an optimal case where the analogy factor defined by the heat transfer and the skin-friction drag is maximized, the parameter sets agree well with those predicted by the feedback control used in optimal and sub-optimal control theories (Hasegawa et al., 2011; Yamamoto et al., 2013). Hence, the traveling wave induces skin-friction drag reduction effect, relaminarization phenomenon, and the dissimilar control effect. However, the investigations are performed in turbulent channel or pipe flows. Conversely, in the present study, the control effect is investigated in turbulent Taylor–Couette flows (referred as TC flows, hereafter).

A TC flow is a flow in gaps between concentric annular cylinder and is considered as a canonical flow in fluid dynamics. Taylor (1923) pioneered the research on TC flow, and this was followed by numerous studies e.g., categorization of the flow pattern (Andereck et al.1986), the behavior of the flow pattern with the increase of the Reynolds number (Coles, 1965; Fenstermacher, 1979; Lathrop et al., 1992a; Lathrop et al., 1992b), quasi-periodicity in the azimuthal direction (Takeda, 1999; Wang et al., 2005), and DNSs of the flow (e.g., Bilson and Bremhorst, 2007; Pirrò and Quadrio, 2007; Dong, 2007). In addition to the flow pattern, heat transfer in the TC flow was also investigated. For example, Kedia et al.(1998) performed a numerical simulation to examine gravitational and centrifugal potentials on the stability of heated and incompressible TC flow. Fènot et al.(2011) reviewed and summarized the relation between Nusselt and Taylor numbers. Teng et al.(2015) performed direct numerical simulations to study the Taylor–Couette flow between two rotating coaxial cylinders in the presence of a radial temperature gradient, and they investigated the effect of buoyancy force on flow patterns. Based on the derivation of Eq. (1) and theoretical analysis by Eckhardt et al.(2007), Ohsawa et al.(2016a) derived the identity equations of torque coefficient C_m and the Stanton number St (of inner cylinder) in the Taylor–Couette flow in the following manner:

$$C_m = \frac{1}{R_o - R_i}\int_{R_i}^{R_o}\left(r^3\frac{\overline{u_r'u_\theta'}}{r} - \frac{r^3}{\mathrm{Re}_c}\frac{\partial}{\partial r}\left(\frac{\overline{u_\theta}}{r}\right)\right)dr, \quad \mathrm{St}_i = \frac{1}{R_i\,(R_o - R_i)}\int_{R_i}^{R_o}\left(r\overline{u_r'T'} - \frac{r}{\mathrm{Re}_c\mathrm{Pr}}\frac{\partial\overline{T}}{\partial r}\right)dr. \tag{2}$$

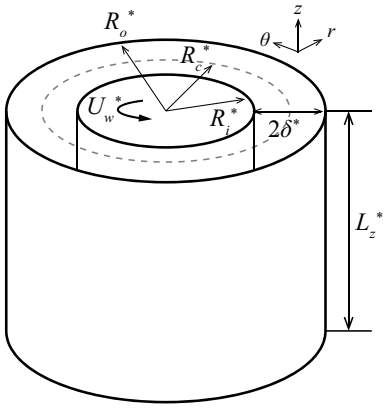

Fig. 1 The TC flow and coordinate systems.

Specifically, R_o and R_i denote the radii of the outer and inner cylinders, r denotes the radial coordinate, $\overline{u_r' u_\theta'}$ and $\overline{u_r' T'}$ denote the Reynolds shear stress and turbulent heat flux, respectively, $\overline{u_\theta}$ and $\overline{T}$ denote mean radial velocity and temperature, respectively. The effect of curvature appears in the former equation: the curvature affects Reynolds shear stress and the mean shear. It assumed therefore that the dissimilarity between momentum and energy transfer may become large if the curvature is large (or a gap between cylinder is large). Ohsawa et al.(2016a) estimated the contribution of each term to the torque and heat transfer coefficients and extended the equation into Taylor-Couette-Poiseuille flow (Ohsawa et al., 2016b).

Thus, the objective of the present study is to investigate the torque reduction effect and also the heat transfer effect by a traveling wave-like blowing and suction in the turbulent TC flow. A parametric study for control parameters of the traveling wave is expected to demonstrate a range of the torque reduction and heat transfer enhancement. The TC flow differs from the Poiseuille flow, e.g., the Taylor vortex appears, the driving force is the wall velocity, a wall curvature exists, and the TC flow includes many modes based on the parameters (Grossmann et al., 2016). Additionally, similarity exists in the boundary condition: wall velocity and temperature on the inner cylinder are set as one and those on the outer cylinder are set to zero. A preliminary DNS of the TC flow controlled by the traveling wave under several sets of parameters was reported by Ogino et al.(2019). Thus, the present study is an extension of the study by Ogino et al.(2019). Specifically, Ogino et al.(2019) only investigated the torque reduction effect on the TC flow, while in the present study, we consider the energy equation to focus on heat transfer.

The study is structured as follows: in sec. 2, the details of DNS and computational conditions are summarized; in sec. 3, we present the simulation results and discussion; and in sec. 4, we present our conclusions.

2. Direct Numerical simulation

Figure 1 shows a schematic of the TC flow. An asterisk denotes a dimensional variable. The radii of the inner and outer cylinders are denoted as R_i^* and R_o^*, respectively. A half gap between the cylinders $((R_o^* - R_i^*)/2)$ is denoted by δ^*. The ratio between the inner and outer cylinder radii is $\xi = 0.882$.

The length of the computational domain in the z-direction is L_z^*. A periodic condition is imposed in the axial direction. The inner cylinder rotates, while the outer cylinder is immobile. A no-slip condition is imposed on the inner and outer walls (except the control input). The inner and outer wall temperatures ($T_{w,i}$ and $T_{w,o}$) are set as 1 and zero, respectively. The governing equations used for the simulation are incompressible continuity, Navier-Stokes, and energy equations. The continuity equation is

$$\frac{1}{r}\frac{\partial}{\partial r}(ru_r) + \frac{1}{r}\frac{\partial u_\theta}{\partial \theta} + \frac{\partial u_z}{\partial z} = 0, \tag{3}$$

where u is the velocity and r, θ, and z represent the radial, azimuthal, and axial directions, respectively. The Navier-Stokes and energy equations are

$$\frac{\partial u_r}{\partial t} = -\left(\frac{1}{r}\frac{\partial}{\partial r}ru_r u_r + \frac{1}{r}\frac{\partial}{\partial \theta}u_\theta u_r + \frac{\partial}{\partial z}u_z u_r - \frac{u_\theta^2}{r}\right) - \frac{\partial p}{\partial r} + \frac{1}{\mathrm{Re}_c}\left(\frac{1}{r}\frac{\partial}{\partial r}\left(r\frac{\partial u_r}{\partial r}\right) - \frac{u_r}{r^2} + \frac{1}{r^2}\frac{\partial^2 u_r}{\partial \theta^2} + \frac{\partial^2 u_r}{\partial z^2} - \frac{2}{r^2}\frac{\partial u_\theta}{\partial \theta}\right),$$

Table 1 Verification of the uncontrolled flow.

Domain	(N_r, N_θ, N_z)	L_z^*	$C_{f,i} \times 10^3$	$C_{f,o} \times 10^3$	$\mathcal{T} \times 10^{-7}$	$\mathrm{St}_i \times 10^3$	$\mathrm{St}_o \times 10^3$
Domain S	(128, 512, 256)	$5\delta^*$	2.67	2.09	5.22	1.81	1.61
Domain M	(128, 512, 512)	$10\delta^*$	2.69	2.11	5.27	2.01	1.78
Domain L	(128, 512, 768)	$15\delta^*$	2.70	2.10	5.26	2.03	1.80
Domain MF	(256, 512, 512)	$10\delta^*$	2.69	2.13	5.31	2.01	1.78

$$\frac{\partial u_\theta}{\partial t} = -\left(\frac{1}{r}\frac{\partial}{\partial r}ru_r u_\theta + \frac{1}{r}\frac{\partial}{\partial \theta}u_\theta u_\theta + \frac{\partial}{\partial z}u_z u_\theta + \frac{u_r u_\theta}{r}\right) - \frac{1}{r}\frac{\partial p}{\partial \theta} + \frac{1}{\mathrm{Re}_c}\left(\frac{1}{r}\frac{\partial}{\partial r}\left(r\frac{\partial u_\theta}{\partial r}\right) - \frac{u_\theta}{r^2} + \frac{1}{r^2}\frac{\partial^2 u_\theta}{\partial \theta^2} + \frac{\partial^2 u_\theta}{\partial z^2} + \frac{2}{r^2}\frac{\partial u_r}{\partial \theta}\right),$$

$$\frac{\partial u_z}{\partial t} = -\left(\frac{1}{r}\frac{\partial}{\partial r}ru_r u_z + \frac{1}{r}\frac{\partial}{\partial \theta}u_\theta u_z + \frac{\partial}{\partial z}u_z u_z\right) - \frac{\partial p}{\partial z} + \frac{1}{\mathrm{Re}_c}\left(\frac{1}{r}\frac{\partial}{\partial r}\left(r\frac{\partial u_z}{\partial r}\right) + \frac{1}{r^2}\frac{\partial^2 u_z}{\partial \theta^2} + \frac{\partial^2 u_z}{\partial z^2}\right),$$

$$\frac{\partial T}{\partial t} = -\left(u_r\frac{\partial T}{\partial r} + u_\theta\frac{1}{r}\frac{\partial T}{\partial \theta} + u_z\frac{\partial T}{\partial z}\right) + \frac{1}{\mathrm{Re}_c\mathrm{Pr}}\left(\frac{1}{r}\frac{\partial}{\partial r}\left(r\frac{\partial T}{\partial r}\right) + \frac{1}{r^2}\frac{\partial^2 T}{\partial \theta^2} + \frac{\partial^2 T}{\partial z^2}\right).$$

Here, t is the time and p is the pressure. We employed an inner cylinder velocity U_w^*, radius R_c^*, and an inner cylinder temperature $T_{w,i}^*$ as reference values. The Reynolds number defined by U_w^* and radius $R_c^*(= (R_i^* + R_o^*)/2)$ is set as $\mathrm{Re}_c = 84{,}000$, and a Prandtl number is set to as Pr=0.71. All simulations begin from a fully developed turbulent TC flow. The flow field was calculated using a DNS code discretized by the energy conservative finite difference method (Fukagata and Kasagi, 2002). A staggered grid system is employed: pressure is defined at the center of the cell while velocities are defined on the face of the cells. The mesh size is uniform in the axial and azimuthal directions and is non-uniform in the wall-normal direction.

To validate the computational domain size and grid resolution, we compare results in uncontrolled flow on four different runs, as shown in Table 1. Specifically, Domain S, Domain M, and Domain L are small, middle, and large computational domains ($L_z^* = 5\delta^*$, $10\delta^*$, and $15\delta^*$), respectively. Because the reference length is R^*, the axial length of the system is $L_z = 0.6264$ in Domain M. Although the grid resolution is common, Domain MF exhibits $L_z^* = 10\delta^*$, albeit higher grid resolution in the r-direction. Furthermore, the skin-friction coefficient C_f, torque $\mathcal{T}$, and Stanton number St are defined as,

$$C_f = \frac{\tau_w^*}{\frac{1}{2}\rho^* U_w^{*2}} = \frac{2}{\mathrm{Re}_c}\left(r\frac{\partial}{\partial r}\left(\frac{\overline{u_\theta}}{r}\right)\right)_w, \tag{4}$$

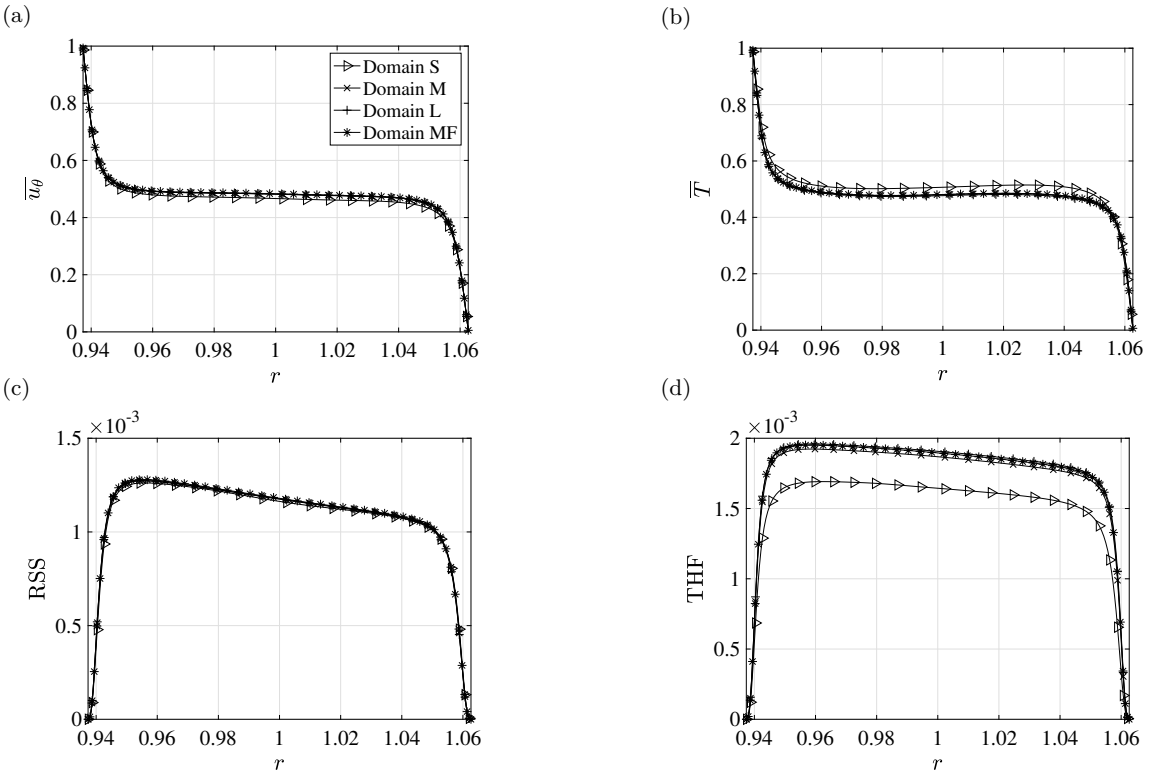

Fig. 2 Flow statistics of the uncontrolled TC flow: (a) $\overline{u_\theta}$, (b) $\overline{T}$, (c) $\overline{u_r' u_\theta'}$, and (d) $\overline{u_r' T'}$.

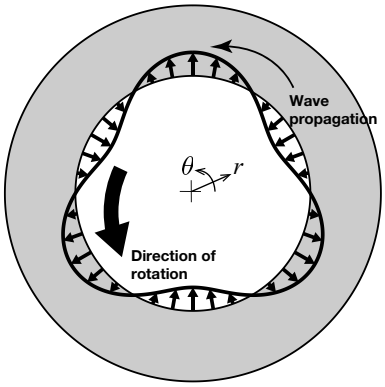

Fig. 3 The traveling wave (top view of the cylinder).

$$\mathcal{T} = \mathrm{Re}_c R_i \left(r \frac{\partial}{\partial r} \left(\frac{\overline{u_\theta}}{r} \right) \right)_i 2\pi R_i = \mathrm{Re}_c R_o \left(r \frac{\partial}{\partial r} \left(\frac{\overline{u_\theta}}{r} \right) \right)_o 2\pi R_o, \tag{5}$$

$$\mathrm{St} = \frac{h^*}{c_p^* \rho^* U_w^*} = \frac{1}{\mathrm{Re}_c \mathrm{Pr}} \left(\frac{\partial \overline{T}}{\partial r} \right)_w, \tag{6}$$

where, τ_w^*, c_p^*, and h^* denote wall-shear stress, specific heat capacity, and heat transfer coefficient, respectively. The bar denotes the temporal and spatial average,

$$\overline{f} = \frac{1}{\mathscr{T} 2\pi L_z} \int_0^{\mathscr{T}} \int_0^{2\pi} \int_0^{L_z} f dz d\theta dt, \tag{7}$$

where, f denotes an arbitrary and $\mathscr{T}$ denotes an averaging time. The fluctuation from $\overline{f}$ is denoted by the prime, i.e., $f = \overline{f} + f'$. The heat transfer is balanced between inner and outer walls i.e., $\mathrm{St}_i = \mathrm{St}_o R_o / R_i$. With the exception of lower St in Domain S, C_f, $\mathcal{T}$, and St are almost constant irrespective of the computational domain. Racina and Kind (2006) preformed an experimental study of the turbulent TC flow and derived an empirical formula for torque $\mathcal{T}_{emp}$ as follows:

$$\mathcal{T}_{emp} = 0.113 \frac{\xi^{3/2}}{(1-\xi)^{7/4}} \mathrm{Re}_\delta^{1.764}. \tag{8}$$

In the present numerical condition, the empirical torque is $\mathcal{T}_{emp} = 4.91 \times 10^7$: it differs from the computational result $\mathcal{T}$; however, this difference is small, and the agreement is reasonable.

The statistics in the uncontrolled TC flow for different computational domains are compared in Fig. 2: the mean velocity $\overline{u_\theta}$, Reynolds shear stress (referred as RSS, hereafter), mean temperature $\overline{T}$, and turbulent heat flux (THF). The results indicate that the difference among statistics in each domain is extremely small with the exception of $\overline{T}$ and the THF in Domain S. In the following section, Domain S is employed for the parametric study to decrease the computational cost in Sec. 3.1; Domain M is employed to investigate control effects in detail in Sec. 3.2.

3. Results and discussion

3.1. Parametric study

Traveling wave-like blowing and suction are employed as the flow control technique. Figure 3 shows a top view of the TC flow with the traveling wave-like blowing and suction. The traveling wave is applied to the inner cylinder and is homogeneous in the z-direction as follows:

$$u_{r,i} = a \cos\left(k(\theta - ct)\right), \tag{9}$$

where, $u_{r,i}$ denotes the wall-normal velocity on the inner cylinder. The control parameters include the amplitude of the wave a, wavenumber k, and wavespeed c. The positive and negative values of c indicate that the wave travels in the co-rotating and counter-rotating directions of the inner cylinder, respectively. The amplitude of the wave is fixed at $a = 0.1$.

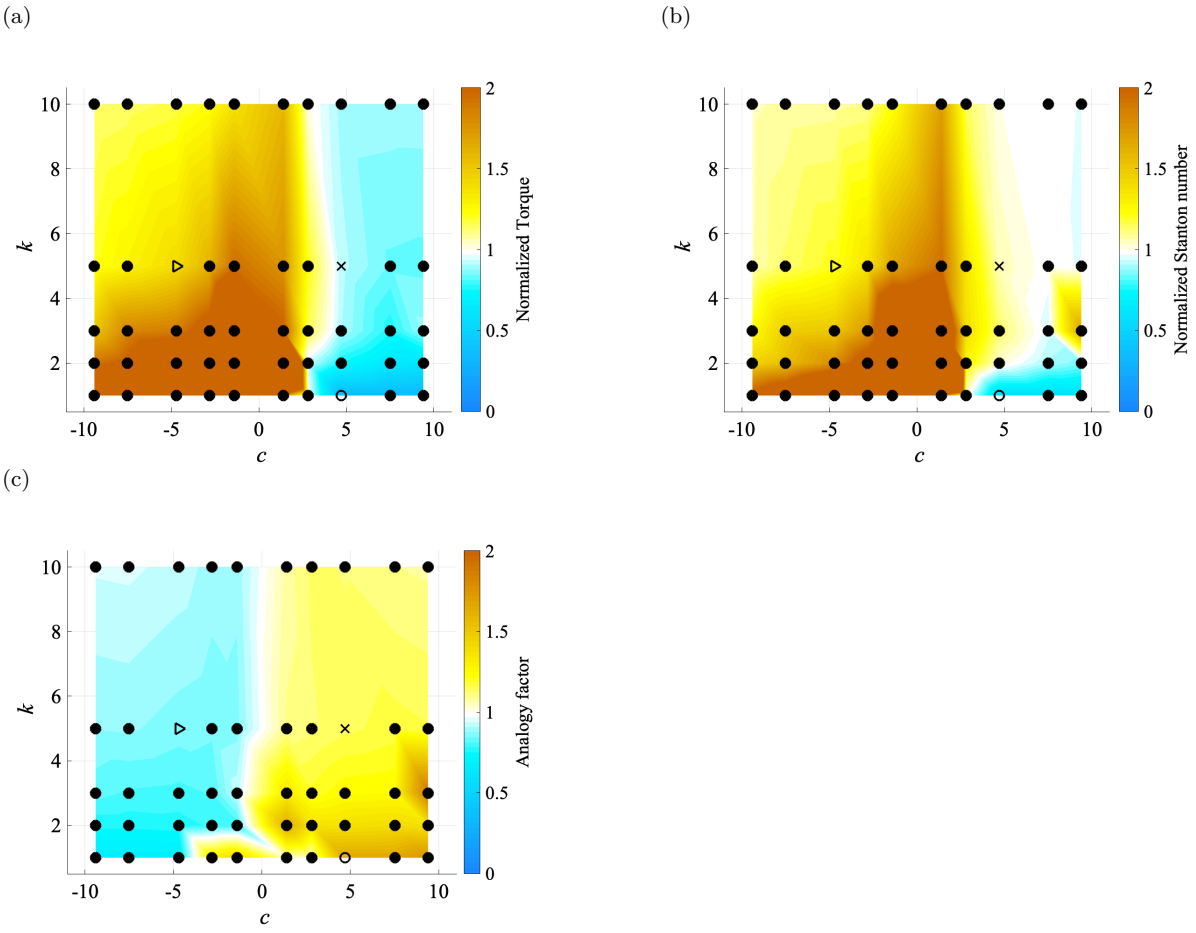

Fig. 4 (a) Torque, (b) Stanton number, and (c) analogy factor at inner wall in Domain S. The unit corresponds to those in the uncontrolled case. The markers denote a single computational run: ▹, Case 1; ∘, Case 2; ×, Case 3.

The control effect is investigated in a wider range of the control parameters: $-9.6 < c < 9.6$ and $1 < k < 10$. We employed Domain S to reduce the computational cost. Figure 4 shows the torque and Stanton number normalized by those in uncontrolled flow. It depicts that a torque lower than the unit value indicates torque reduction; a Stanton number exceeding the unit value indicates heat transfer enhancement. The single marker denotes a simulation (▹, ∘, and × denote reference cases in Sec. 3.2). The torque decreases at $c > 3.2$, where the wave travels in the corotating direction and its wavespeed exceeds the wall velocity of the inner cylinder. At $c > 4.8$ and $k = 1$, the torque decreases by 60%. The Stanton number is similar to the torque while some parameter sets are different. For example, at $c = 4.8$ and $k > 2$, the Stanton number is higher. However, the torque is lower than the unit value, thereby indicating that a reduction in torque and enhancement in heat transfer are realized simultaneously. Hence, torque and the heat transfer are affected by the wavenumber and wavespeed of the traveling wave. In the following section, we select three case and they are indicated by markers in Fig. 4: ▹ (Case 1) denotes the heat transfer enhancement case (but torque also increases); ∘ (Case 2) denotes the relaminarization case; and × (Case 3) denotes the dissimilar case. Figure 4(c) shows an analogy factor based on the friction coefficient and the Stanton number on the inner cylinder wall. The analogy factor is defined as $A = 2\mathrm{St}_i\mathrm{Pr}^{2/3}/C_{f,i}$. The factor is $A = 1.04$ in the uncontrolled flow and the momentum transfer is almost comparable to the energy transfer. We guess therefore that the effect of the cylinder curvature on the dissimilarity is small. Positive analogy factor is obtained by the corotating wave and the count-rotating wave at $c > -2.82$ and $k = 1$. In Case 1, the analogy factor is negative. In Case 2, the analogy factor is positive, where the skin-friction drag much decreases due to the relaminarization phenomenon. In Case 3, the analogy factor is positive due to the reduction of the skin-friction (or torque) and the increase of the heat transfer. The analogy factor shows a similar trend in terms of wavenumber to that in a plane channel flow (Kaithakkal et al., 2020). However, a large peak is observed at large and positive c and it seems to be effect of the current curved flow.

Table 2 Control performance of reference cases in Domain M.

Case	(a, c, k)	$C_{f,i} \times 10^3$	$C_{f,o} \times 10^3$	$\mathcal{T} \times 10^{-7}$	$\mathrm{St}_i \times 10^3$	$\mathrm{St}_o \times 10^3$
Case NC	$(-, -, -)$	2.69	2.11	5.27	2.01	1.78
Case 1	$(0.1, -4.8, 5)$	3.84	3.00	7.50	2.51	2.23
Case 2	$(0.1, 4.8, 1)$	1.03	0.88	2.11	1.24	1.03
Case 3	$(0.1, 4.8, 5)$	2.45	1.94	4.83	2.14	1.89

Table 3 Control performance of reference cases in Domain S and Domain M.

	Domain S		Domain M	
Case	$\mathcal{T}/\mathcal{T}_{NC}$	$\mathrm{St}_i/\mathrm{St}_{i,NC}$	$\mathcal{T}/\mathcal{T}_{NC}$	$\mathrm{St}_i/\mathrm{St}_{i,NC}$
Case 1	1.41	1.19	1.42	1.25
Case 2	0.35	0.56	0.40	0.62
Case 3	0.92	1.05	0.92	1.06

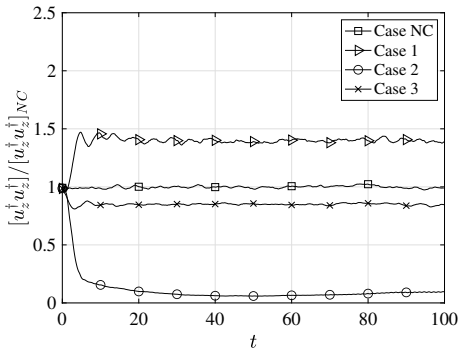

Fig. 5 Time trace of $\left[u_z^\dagger u_z^\dagger\right]$ normalized by the uncontrolled value.

3.2. Control effect

The control effect of traveling wave on the TC flow is discussed in detail. As shown in Table 2, three cases are selected as references and their control performance are summarized. The control performance is averaged in time at $80 < t < 100$. Furthermore, Case NC is uncontrolled flow case. Case 1 denotes the counter-rotating traveling wave with the short wavelength: the heat transfer and torque are increased. Case 2 denotes the co-rotating traveling wave with the long wavelength: large reduction in drag is obtained and the heat transfer is lower than that of the uncontrolled flow. The relaminarization phenomena occurs here. Case 3 denotes the co-rotating traveling wave with short wavelength: torque decreases while heat transfer is enhanced where the similarity between the momentum and heat transfer ceases. Table 3 compares the control performance in Domain S and Domain M. The subscript of NC means the uncontrolled flow. The discrepancy in control performance is found, but the trend is unchanged.

The time trace of the velocity fluctuation in the axial direction is discussed to support the result in Case 2. Figure 5 shows the time trace of $\left[u_z^\dagger u_z^\dagger\right]$ normalized by the uncontrolled value. The dagger † denotes the instantaneous velocity fluctuation from spatial average, and it is defined as

$$f^\dagger = f - \frac{1}{2\pi r L_z} \int_0^{L_z} \int_0^{2\pi} f r d\theta dz. \tag{10}$$

Specifically, f denotes the arbitrary function. Additionally, the parenthesis [] denotes the integration over the entire computational domain, as

$$[f] = \frac{1}{\pi(R_o^2 - R_i^2)L_z} \int_0^{L_z} \int_0^{2\pi} \int_{R_i}^{R_o} f r dr d\theta dz. \tag{11}$$

The control input denotes the wall-normal velocity on the inner cylinder surface, and thus radial velocity is directly created and azimuthal velocity is created via continuity. Conversely, axial velocity $u_z^\dagger$ is not directly affected, and thus, the volume averaged $u_z^\dagger u_z^\dagger$ reflects the existence of the turbulence and the Taylor vortex. The results indicated that the volume averaged $u_z^\dagger u_z^\dagger$ in Case 2 significantly decreases when compared with that of Case NC, and the relaminarization phenomenon occurs. The remaining and small $[u_z^\dagger u_z^\dagger]$ corresponds to the remained velocity fluctuation as shown in Fig. 6(e-f) (shown later). Additionally, when compared to Case NC,

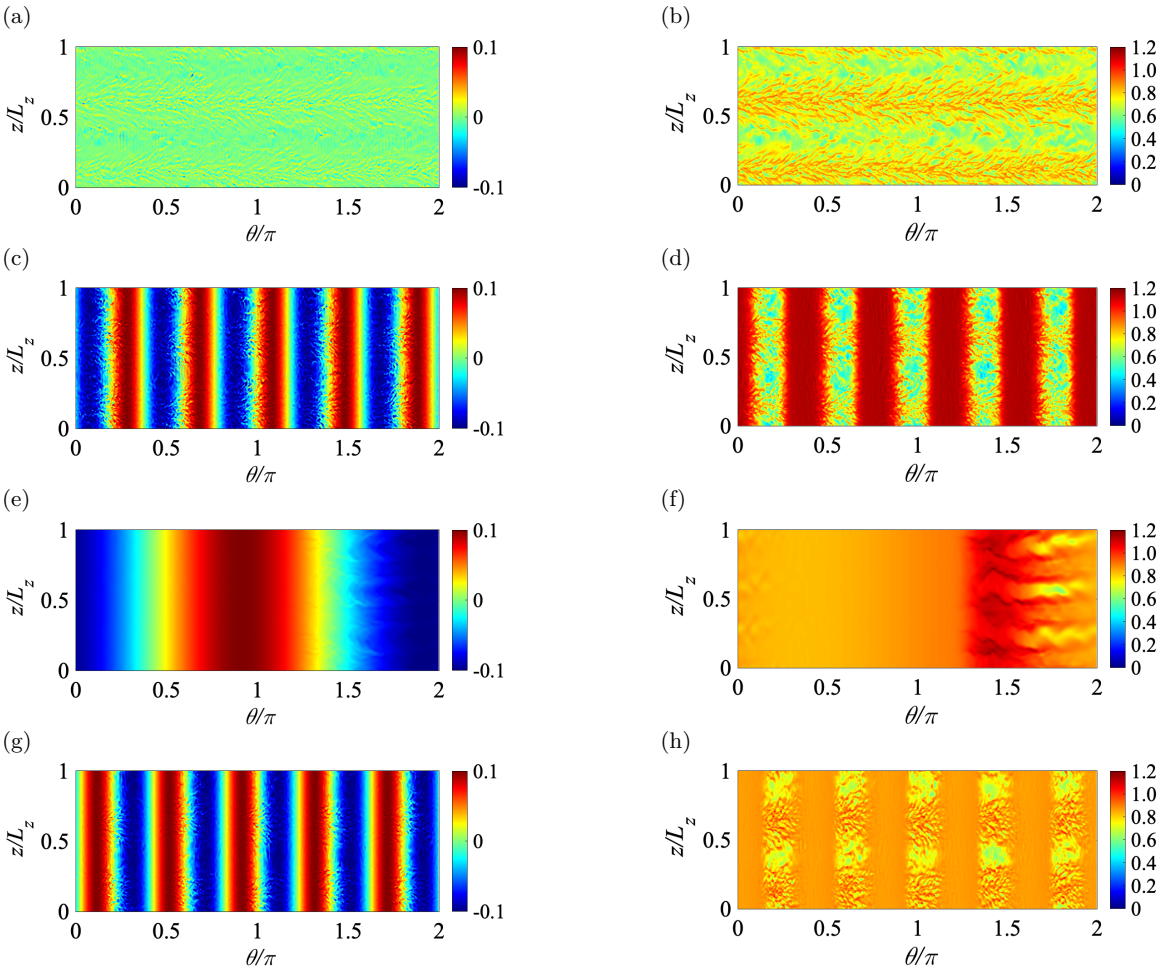

Fig. 6 Instantaneous flow field on θ-z plane at $y^+ \approx 7.5$ ($y = r - R_i$) and $t = 100$: left column, u_r; right column, u_θ: (a-b) Case NC, (c-d) Case 1, (e-f) Case 2, and (g-h) Case 3. The axial length is $L_z = 0.6264$.

$\left[u_z^\dagger u_z^\dagger\right]$ is higher in Case 1 and is lower in Case 3. Hence, these reflect the increase or decrease in the turbulence and Taylor-vortex by the traveling wave, as discussed subsequently.

The instantaneous flow field of u_r and u_θ on a θ-z plane at $y^+ \approx 7.5$ and $t = 100$ is shown in Fig. 6. Specifically, y^+ is defined as the distance from the inner wall and is nondimensionalized by the friction velocity on the inner wall. We note that the friction Reynolds number corresponds to 192 for inner wall and 170 for outer wall in the uncontrolled flow. In Case NC, u_r is very low due to the effect of the wall. The fluctuation in u_θ gathers and creates Herringbone streaks (Dong, 2007). Herringbone streaks appear where the upward flow from the inner wall is generated by the Taylor vortex. Conversely, the fluctuation of u_θ is weakened at the downward flow region of the Taylor vortex. In Case 1, the traveling wave creates the positive and negative u_r alternating in the θ-direction. Specifically, the wave travels in the negative θ-direction. The radial velocity u_r is disturbed at the interface from negative to positive u_r (e.g., $\theta/\pi \approx 0.5$). The large and small u_θ regions alternate in the streamwise direction, which is due to the direct effect of the traveling wave. The wave travels in the negative θ direction, and thus the injected fluid flow from the blowing part of the traveling wave is sucked into the suction part downstream of the wave. Therefore, the flow is accelerated locally. This is observed in the channel flow (Hœpffner and Fukagata, 2008) and pipe flow (Koganezawa et al., 2019). Additionally, Herringbone streaks are observed at the small u_θ region, and thus it implies the existence of the Taylor vortex. In Case 2, the wave travels in the positive direction, and the wavelength exceeds those of other cases. Velocity fluctuation is observed at $\theta/\pi > 1.5$. However, Herringbone streaks are not observed in contrast to other cases. In Case 3, the wavelength is the same as that in Case 1, and the wave travels in the positive θ direction. Given blowing and suction from the wall, the local acceleration of u_θ occurs. However, it is lower than that in Case 1. Additionally, the Herringbone streaks are observed in u_θ, and its amplitude exceeds those in Case NC and Case 1.

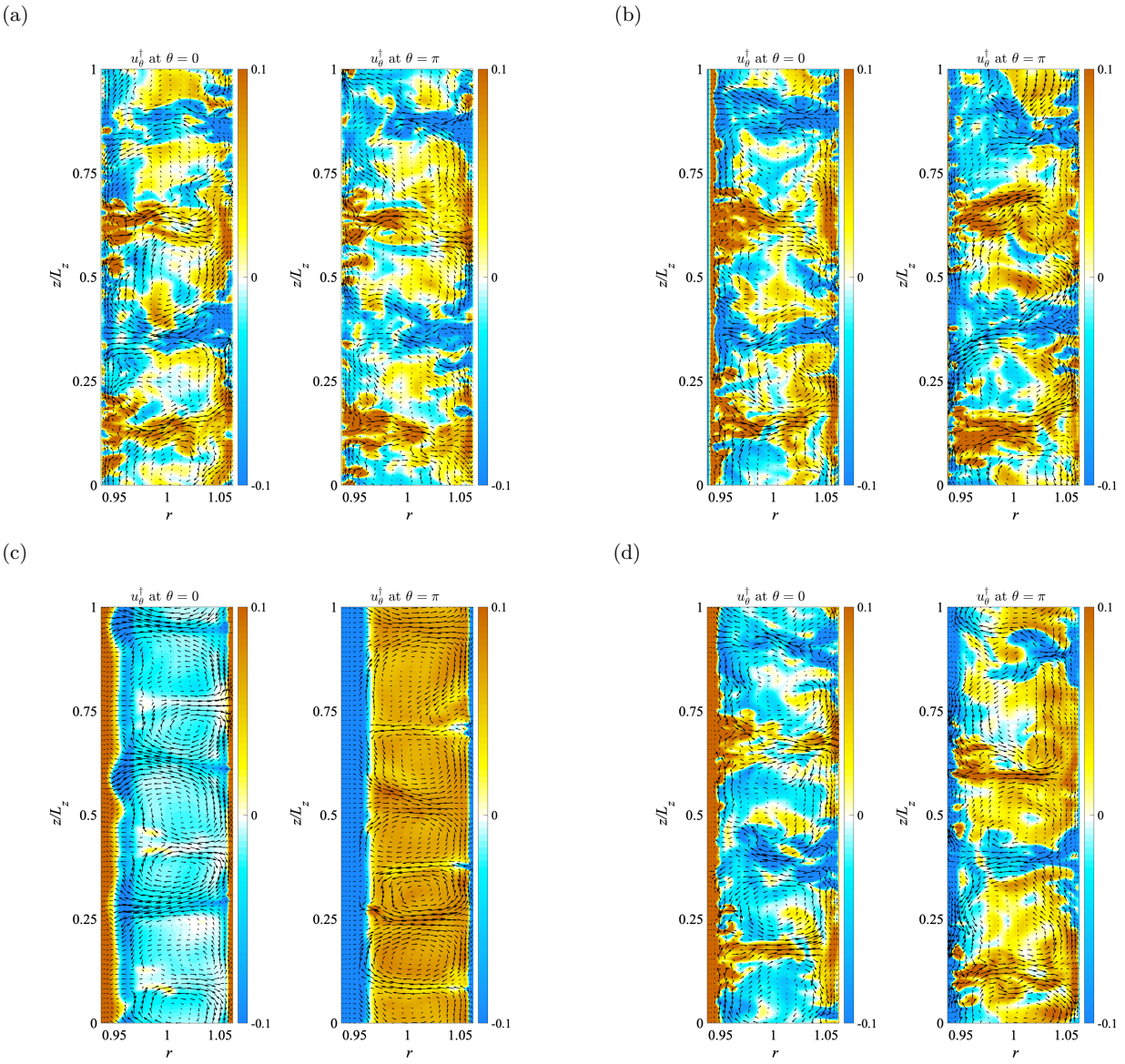

Fig. 7 Instantaneous flow field on r-z plane: (a) Case NC, (b) Case 1, (c) Case 2, and (d) Case 3. The color shows $u_\theta^\dagger$. The axial length is $L_z = 0.6264$.

The above observation suggests that the creation of the local flow acceleration region is a direct effect of the traveling wave. Furthermore, the wave indirectly affects the Taylor vortex i.e., the Herringbone streaks are observed although they are weakened and promoted in Case 1 and Case 3, respectively. However, in the relaminarization phenomena (Case 2), the direct effect appears, and the Herringbone streaks are not observed in the region near the inner cylinder.

Figure 7 shows the instantaneous flow field on r-z plane to demonstrate the Taylor-vortex under the traveling wave. The inner wall is rotated by $U_w = 1$ and heated at $T = 1$, while the outer wall is immobile and cooled at $T = 0$. In Case NC, two pairs of Taylor-vortex appear although they are distorted. The u_θ is pushed-up from the wall where the velocity fluctuates. The Taylor-vortices in Cases 1 and 3 are similar to that in Case NC with the exception of the region near the inner wall. In Case 2, the velocity fluctuation significantly decreases, and three pairs of the Taylor-vortices are observed. Mamori et al.(2010) investigated that the influence layer by the traveling wave-like blowing and suction in the channel flow is scaled by the combination of the wavespeed, wavenumber, and the Reynolds number (i.e., $\sqrt{|c|\,k\mathrm{Re}}$). This scaling is based on the analogy of the Stokes' second problem. According to them, given the long wavelength of the traveling wave in the present DNS, the region affected by the traveling wave becomes thick and the influence layer thickness becomes increases. Therefore, the region of $|u_\theta| \approx \pm 0.1$ without fluctuation appears near the inner cylinder.

3.3. Three-component decomposition

Three-component decomposition is introduced to understand the contribution from the traveling wave to the TC flow. In previous studies, decomposition is used to distinguish contributions from the direct effect and indirect effect from the traveling wave (Mamori et al., 2014; Kaithakkal et al., 2020). Ogino et al.(2019) employed the three-component decomposition to distinguish them in the TC flow and concluded that the contribution from the coherent component on the torque was small. Conversely, the TC flow includes the TC vortex, and the aim of the study is to investigate the effect of the traveling wave. Therefore, we define the three-component decomposition to distinguish the TC vortex and other components. For an arbitrary quantity f, the three-component decomposition is defined as

$$f = \overline{f} + \tilde{f} + f''. \tag{12}$$

The tilde and double prime are termed as the advection and turbulent components, respectively. The bar denotes the spatial and time average and is defined in Eq. (7), and azimuthal and temporal average is defined as

$$\langle f \rangle(r,z) = \frac{1}{\mathscr{T} 2\pi} \int_0^{\mathscr{T}} \int_0^{2\pi} f(r,z,\theta,t) d\theta dt \tag{13}$$

Therefore, a relation exists between the bar and parenthesis as follows:

$$\overline{f} = \frac{1}{L_z} \int_0^{L_z} \langle f \rangle dz. \tag{14}$$

Hence, f is expressed as follows:

$$f = \overline{f} + f' = \langle f \rangle + f'' = \overline{f} + \tilde{f} + f''. \tag{15}$$

Based on the present three component decomposition, the RSS and THF are decomposed as follows:

$$\overline{u_r' u_\theta'} = \overline{\tilde{u}_r \tilde{u}_\theta} + \overline{u_r'' u_\theta''}, \quad \overline{u_r' T'} = \overline{\tilde{u}_r \tilde{T}} + \overline{u_r'' T''}. \tag{16}$$

The former term is designated as the advection component and corresponds to the contribution from the Taylor-vortex; the latter term denotes the turbulent component and corresponds to the turbulence, including the direct effect, of the traveling wave. The sum of the advection and turbulent components are termed as the total component.

Figure 8 shows $\tilde{u}_r \tilde{u}_\theta$, $\langle u_r'' u_\theta'' \rangle$, $\tilde{u}_r \tilde{T}$, and $\langle u_r'' T'' \rangle$, with the velocity vector of $\tilde{u}_r$ and $\tilde{u}_\theta$ on the $r-z$ plane. In Case NC, two pairs of the Taylor vortex are clearly observed. The positive and large $\tilde{u}_r \tilde{u}_\theta$ is created at the interface of the Taylor- vortex, where the upward flow from the cylinder wall is induced. The positive $\langle u_r'' T'' \rangle$ is observed at the upward flow region and also near the wall region. A similar distribution is observed in $\tilde{u}_r \tilde{T}$ and $\langle u_r'' T'' \rangle$. In Case 1, each component increases when compared to that in Case NC, and this corresponds to the increase in the friction drag and heat transfer. In Case 2, the Taylor-vortices are lower than that in Case NC and pushed up from the inner wall cylinder. It should be noted that the advection components ($\tilde{u}_r \tilde{u}_\theta$ and $\tilde{u}_r \tilde{T}$) are almost zero or significantly lower than the turbulent components ($\langle u_r'' u_\theta'' \rangle$ and $\langle u_r'' T'' \rangle$). In Case 3, the distributions are almost identical to those in Case NC.

We note that the Taylor vortex stays at the same location during the integration time in the present study, while there is no guarantee that the Taylor vortex stays at the same location for a long time. However, the present three-component decomposition is possible if a phase-lock average is employed: a phase-lock average means that an averaging frame is moved in accordance with the convection of the Taylor vortex.

Figure 9 shows the RSS and the THF. In Case NC, the advection component exceeds the turbulent component in the RSS and THF with the exception of the near wall region. The turbulent components exhibit peaks in the region near the wall. In Case 1, the total components exceed those in Case NC: the advection and turbulent components increase, and this implies that the Taylor vortex and the turbulence are activated. In the region near the inner wall, two peaks appear in turbulent RSS and THF: the first peak from the inner wall is directly created by the traveling wave (Mamori et al., 2010; Mamori et al., 2014), and the second peak corresponds to the inner peak in Case NC, although it increases. In Case 2, the total components significantly decrease: the advection components are almost zero or very low, and the total component consists of the turbulent component. These correspond to the decreases in the TC vortex and remainder of the turbulence, as

(a)

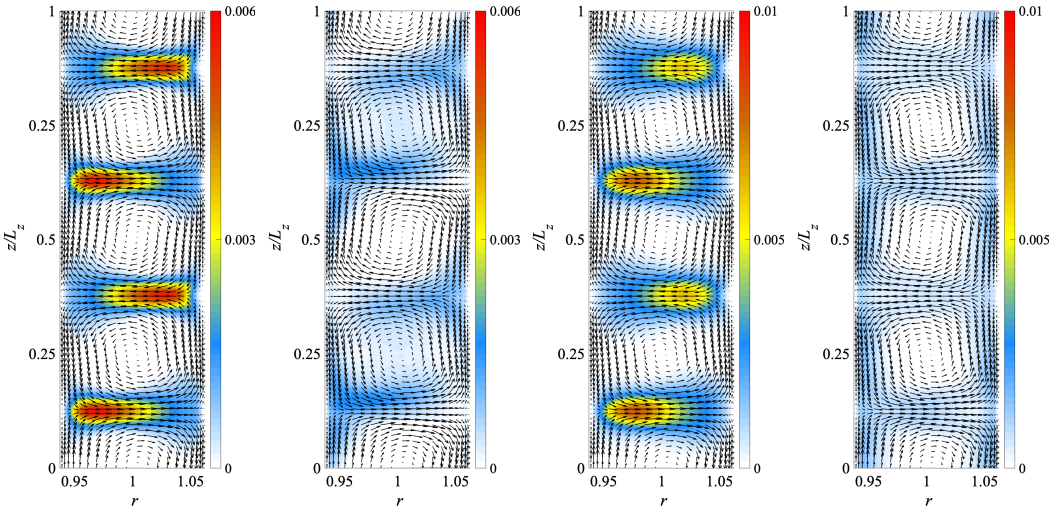

(b)

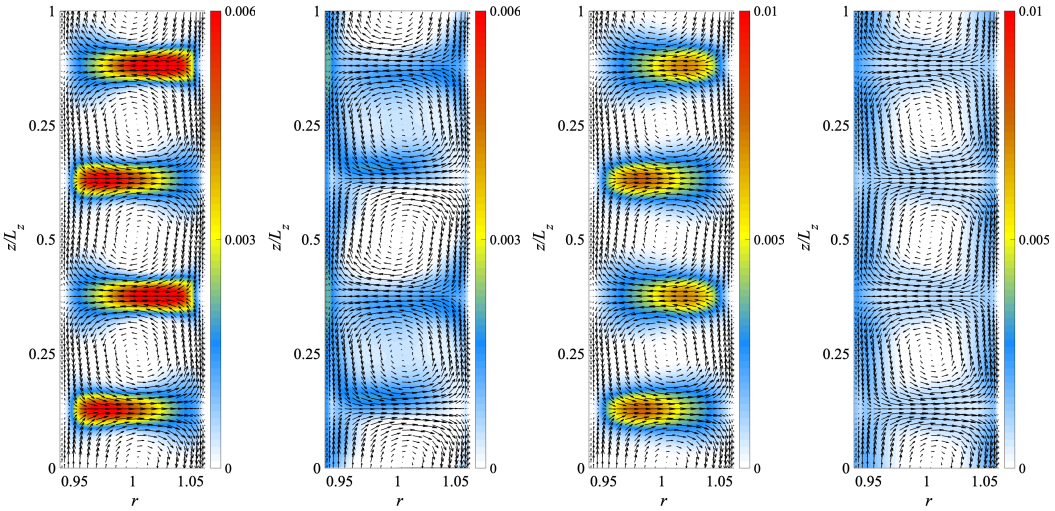

Fig. 8 Distributions of advection-RSS, turbulence-RSS, advection-THF, and turbulence-THF (from left to right): (a) Case NC, (b) Case 1, (c) Case 2, (d) Case 3. The velocity vector is displayed by $\tilde{u}_r$ and $\tilde{u}_\theta$.

shown in Fig. 8. In Case 3, when compared to that in Case NC, the advection RSS slightly decreases whereas the turbulent THF increases in the region near the inner cylinder.

To clarify the quantitative contribution of each component on the torque and heat transfer, the identity equation derived by Ohsawa et al.(2016a) is employed. The identity equations applied by the three-component decomposition are as follows:

$$C_m = \frac{1}{R_o - R_i}\int_{R_i}^{R_o}\left(r^3\frac{\overline{\tilde{u}_r\tilde{u}_\theta}}{r} + r^3\frac{\overline{u_r''u_\theta''}}{r} - \frac{r^3}{\mathrm{Re}_c}\frac{\partial}{\partial r}\left(\frac{\overline{u}_\theta}{r}\right)\right)dr, \tag{17}$$

$$\mathrm{St}_i = \frac{1}{R_i\,(R_o - R_i)}\int_{R_i}^{R_o}\left(r\overline{\tilde{u}_r\tilde{T}} + r\overline{u_r''T''} - \frac{r}{\mathrm{Re}_c\mathrm{Pr}}\frac{\partial\overline{T}}{\partial r}\right)dr. \tag{18}$$

Specifically, C_m denotes the torque coefficient defined as

$$C_m = \frac{\mathcal{T}^*}{\rho^* U_w^* 2\pi R_i^{*2} L_z^*} = \frac{\mathcal{T}}{2\pi\mathrm{Re}_c^2}. \tag{19}$$

The contributions from first, second, and third terms in Eqs. (17) and (18) are termed as the advection, turbulent, and diffusion contributions, respectively, and these contributions are summarized in Table 4. In

(c)

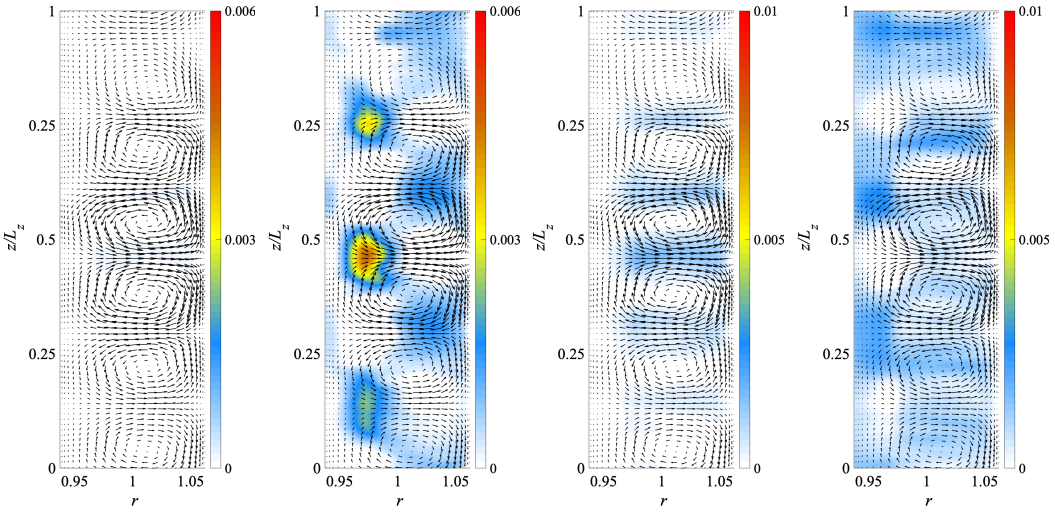

(d)

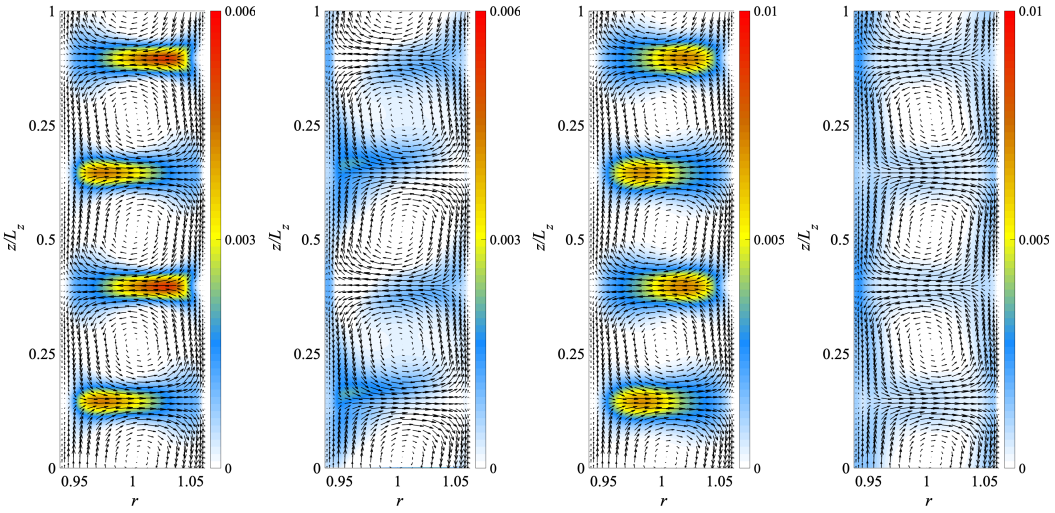

Fig. 8 Continued.

Case NC, the advection contribution significantly contributes to the total C_m and St_i, and the results are in agreement with those in Ohsawa et al.(2016a). In Case 1, all contributions with the exception of the diffusion term increase when compared to those in Case NC. In Case 2, the total C_m and St_i are significantly lower than those in Case NC: the reduction is due to decreases in the advection contribution although the turbulent contribution increases. In Case 3, the total C_m decreases and St_i increases, which results in the dissimilarity between the skin-friction drag and heat transfer: the decrease in C_m is due to the advection contribution; the increase in St_i is due to the decrease in the advection and turbulent contributions. We note that the diffusion term is constant irrespective of the control.

4. Conclusion

In this study, we performed direct numerical simulations of the turbulent Taylor-Couette flows controlled by the traveling wave-like blowing and suction. The results indicated that the traveling wave induces several effects in Taylor–Couette flow as follows: heat transfer enhancement effect, relaminarization phenomenon, and simultaneous achievement of the torque reduction and heat transfer enhancement.

According to the governing and the identity equations, the curvature of the cylinder wall plays the essential role in the dissimilarity of the momentum and energy transfers. The curvature affects the Reynolds shear stress

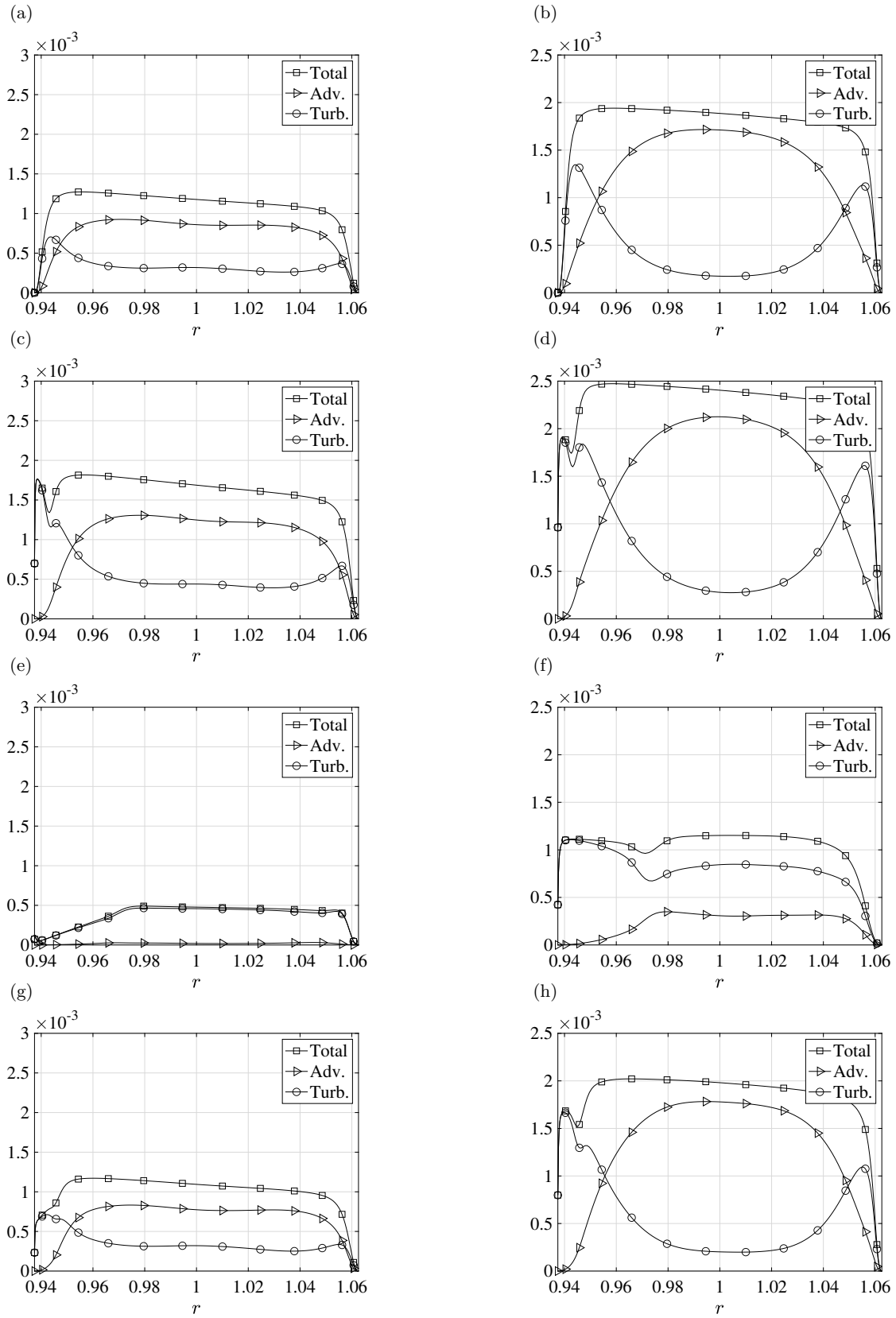

Fig. 9 Reynolds shear stress (left column) and turbulent heat flux (right column): (a-b) Case NC, (c-d) Case 1, (e-f) Case 2, and (g-h) Case 3.

and the shear. In the present DNS, however, the analogy factor of the uncontrolled turbulent flow is 1.04 and the momentum transfer is almost comparable to the energy transfer. It is because the ratio between the inner and outer cylinder radii is not so small (i.e., the curvature is small) and the effect of the curvature on the

Table 4 Contribution to $C_m \times 10^3$ and $\mathrm{St}_i \times 10^3$ in each case.

Case	Total C_m	Advection	Turbulent	Diffusion	Total St_i	Advection	Turbulent	Diffusion
Case NC	1.17	0.76	0.32	0.10	2.01	1.35	0.52	0.14
Case 1	1.69	1.04	0.54	0.10	2.57	1.59	0.83	0.14
Case 2	0.49	0.02	0.37	0.09	1.23	0.25	0.84	0.15
Case 3	1.10	0.67	0.33	0.10	2.14	1.38	0.59	0.14

dissimilarity is small.

The parametric study reveals the range of torque reduction and heat transfer enhancement in the following manner: heat transfer enhancement (with torque increase) occurs when the wave travels in the counter-rotating direction or when it travels in the co-rotating direction at a low wavespeed; the relaminarization phenomenon is observed when the wavenumber is low and the wavespeed exceeds that of the inner cylinder rotation, and a dissimilar control effect is obtained at $c = 4.5$ and $k > 2$. This result may be guideline to design the control of the TC flow.

We selected three parameter sets to clarify the control effect. In the case of the heat transfer enhancement, advection, and turbulent components increase the heat transfer, thereby indicating that the wave affects the Taylor-vortex and other components and promotes their activities. In the relaminarization case, the Taylor-vortex exists although its contribution significantly decreases, while the turbulent contribution remains. In the dissimilar case, the torque reduction is due to decreases in the advection contribution, while heat enhancement is due to advection and turbulent contributions.

Acknowledgments

The study was partially supported by the Ministry of Education, Culture, Sports, Science, and Technology through a Grant-in-Aid for Young Scientists of 19K14884 in 2019.

References

Andereck, C.D., Liu, S.S., and Swinney, H.L., Flow regimes in a circular Couette system with independently rotating cylinders, Journal of Fluid Mechanics, Vol. 164, pp. 155–183 (1986), DOI:10.1017/S0022112086002513.

Bilson, M. and Bremhorst, K., Direct numerical simulation of turbulent Taylor–Couette flow, Journal of Fluid Mechanics, Vol. 579, pp. 227–270 (2007), DOI:10.1017/S0022112007004971.

Chilton, T.H. and Colburn, A.P. Mass transfer (absorption) coefficients prediction from data on heat transfer and fluid friction, Industrial & Engineering Chemistry Research, Vol. 26, pp. 1183–1187 (1934), DOI:10.1021/ie50299a012.

Coles, D., Transition in circular Couette flow, Journal of Fluid Mechanics, Vol. 21, pp. 385–425 (1965), DOI:10.1017/S0022112065000241.

Dong, S., Direct numerical simulation of turbulent Taylor–Couette flow, Journal of Fluid Mechanics, Vol. 587, pp. 373–393 (2007), DOI:10.1017/S0022112007007367

Eckhardt, B., Grossmann, S., and Lohse, D., Torque scaling in turbulent Taylor–Couette flow between independently rotating cylinders, Journal of Fluid Mechanics, Vol. 581, pp. 221–250 (2007), DOI:10.1017/S0022112007005629

Fènot, M., Bertin, Y., Dorignac, E., and Lalizel, G., A review of heat transfer between concentric rotating cylinders with or without axial flow, International Journal of Thermal Sciences, Vol. 50, pp. 1138–1155 (2011), DOI:10.1016/j.ijthermalsci.2011.02.013.

Fenstermacher, P.R., Swinney, H.L., and Gollub, J.P., Dynamical instabilities and the transition to chaotic Taylor vortex flow, Journal of Fluid Mechanics, Vol. 94, pp. 103–128 (1979), DOI:10.1017/S0022112079000963.

Fukagata, K., Iwamoto, K., and Kasagi, N., Contribution of Reynolds stress distribution to the skin friction in wall-bounded flows, Physics of Fluids, Vol. 14, pp. L73–L76 (2002), DOI:10.1063/1.1516779.

Fukagata, K. and Kasagi, N., Highly energy-conservative finite difference method for the cylindrical coordinate system, Journal of Computational Physics, Vol. 181, pp. 478–498 (2002), DOI:10.1006/jcph.2002.7138.

Fukudome, K., Tsukahara, T., and Ogami, Y., Heat and momentum transfer of turbulent stripe in transitional-

regime plane Couette flow, International Journal of Advances in Engineering Sciences and Applied Mathematics, Vol. 10, pp. 291–298 (2018), DOI:10.1007/s12572-018-0219-8.

Grossmann, S., Lohse, D., and Sun, C., High Reynolds number Taylor–Couette turbulence, Annual Review of Fluid Mechanics, Vol. 48, pp. 53–80 (2016), DOI:10.1146/annurev-fluid-122414-034353.

Hasegawa Y. and Kasagi, N., Dissimilar control of momentum and heat transfer in a fully developed turbulent channel flow, Journal of Fluid Mechanics, Vol. 683, pp. 57–93 (2011), DOI:10.1017/jfm.2011.248.

Higashi, K., Mamori, H., and Fukagata, K., Simultaneous control of friction drag reduction and heat transfer augmentation by traveling wave-like blowing/suction, Computational Thermal Sciences: An International Journal, Vol. 3, pp. 521–530, (2011), DOI:10.1615/ComputThermalScien.2011003213.

Hœpffner, J. and Fukagata, K, Pumping or drag reduction? Journal of Fluid Mechanics, Vol. 635, pp. 171–187, (2009), DOI:10.1017/S0022112009007629.

Kaithakkal, A. J., Kametani, Y., and Hasegawa, Y., Dissimilarity between turbulent heat and momentum transfer induced by a streamwise travelling wave of wall blowing and suction, Journal of Fluid Mechanics, Vol. 886, A29 (2020), DOI:10.1017/jfm.2019.1045.

Kasagi, N., Hasegawa, Y., Fukagata, K., and Iwamoto, K., Control of turbulent transport: less friction and more heat transfer, Journal of Heat Transfer, Vol. 134, 031009, 10 pp., (2012), DOI:10.1115/1.4005151.

Kedia. R., Hunt, M. L., and Colonius, T., Numerical simulations of heat transfer in Taylor-Couette flow, Journal of Heat Transfer, Vol. 120, pp. 65–71 (1998), DOI:10.1115/1.2830066.

Koganezawa, S., Mitsuishi, A., Shimura, T., Iwamoto, K., Mamori, H., and Murata, A., Pathline analysis of traveling wavy blowing and suction control in turbulent pipe flow for drag reduction, International Journal of Heat and Fluid Flow, Vol. 77, pp. 388–401 (2019), DOI:10.1016/j.ijheatfluidflow.2019.05.007.

Lathrop, D.P., Fineberg, J., and Swinney, H., Transition to shear-driven turbulence in Couette–Taylor flow, Physical Review A, Vol. 46, pp. 6390–6404 (1992a), DOI:10.1103/PhysRevA.46.6390.

Lathrop, D.P., Fineberg, J., and Swinney, H.L., Turbulent flow between concentric rotating cylinders at large Reynolds number, Physical Review Letters, Vol. 68, pp. 1515–1518 (1992b), DOI:10.1103/PhysRevLett.68.1515.

Lee, C., Min, T., and Kim, J., Stability of a channel flow subject to wall blowing and suction in the form of a traveling wave, Physics of Fluids, Vol. 20, 101513 (2008), DOI:10.1063/1.3006057.

Lieu, B. K. Moarref, R., and Jovanovic, M. R., Controlling the onset of the turbulence by streamwise traveling waves. Part. 2. Direct numerical simulation, Journal of Fluid Mechanics, Vol. 663, pp. 100–119 (2010), DOI:10.1017/S002211201000340X.

Mamori, H., Hœpffner, J., and Fukagata, K, Phase relationship in laminar channel flow controlled by traveling-wave-like blowing or suction, Physical Review E, Vol. 81, 046304 (2010), DOI:10.1103/PhysRevE.81.046304.

Mamori, H. and Fukagata, K., Drag reduction effect by a wave-like wall-normal body force in a turbulent channel flow, Physics of Fluids, Vol. 26, 115104 (2014), DOI:10.1063/1.4901186.

Mamori, H., Iwamoto, K., and Murata, A., Effect of the parameters of traveling waves created by blowing and suction on the relaminarization phenomena in fully developed turbulent channel flow, Physics of Fluids, Vol. 26, 015101 (2014), DOI:10.1063/1.4851256.

Min, T., Kang, S. M., Speyer, J. L., and Kim, J., Sustained sub-laminar drag in a fully developed channel flow, Journal of Fluid Mechanics, Vol. 558, pp. 309–318 (2006), DOI:10.1017/S0022112006000206.

Moarref, R. and Jovanovic, M. R., Controlling the onset of turbulence by streamwise traveling waves. Part 1. Receptivity analysis, Journal of Fluid Mechanics, Vol. 663, pp. 70–99 (2010), DOI:10.1017/S0022112010003393.

Nabae, Y. Kawai, K., and Fukagata, K., Prediction of drag reduction effect by streamwise traveling wave-like wall deformation in turbulent channel flow at practically high Reynolds numbers, International Journal of Heat and Fluid Flow, Vol. 82, 108550 (2020), DOI:10.1016/j.ijheatfluidflow.2020.108550.

Nakanishi, R., Mamori, H., and Fukagata, K., Relaminarization of turbulent channel flow using traveling wave-like wall deformation, International Journal of Heat and Fluid Flow, Vol. 35, pp. 152–159 (2012), DOI:10.1016/j.ijheatfluidflow.2012.01.007.

Ogino, K, Mamori, H., Fukushima, N., Fukudome, K., and Yamamoto, M., Direct numerical simulation of Taylor-Couette turbulent flow controlled by a traveling wave-like blowing and suction, International Journal of Heat and Fluid Flow, Vol. 80, 108463 (2018), DOI:10.1016/j.ijheatfluidflow.2019.108463.

Ohsawa, A., Murata, A., and Iwamoto, K., Contribution of advection, turbulent transport and diffusion terms to Nusselt number and torque coefficient in Taylor-Couette flow, Journal of Thermal Science and Technology, Vol. 11, 16-00350 (2016a), DOI:10.1299/jtst.2016jtst0027.

Ohsawa, A., Murata, A., and Iwamoto, K., Through-flow effects on Nusselt number and torque coefficient in Taylor-Couette-Poiseuille flow investigated by large eddy simulation, Journal of Thermal Science and Technology, Vol. 11, 16-00356 (2016b), DOI:10.1299/jtst.2016jtst0031.

Pirrò, D. annd Quadrio, M., Direct numerical simulation of turbulent Taylor–Couette flow, European Journal of Mechanics - B/Fluids, Vol. 27, pp. 552–566 (2008), DOI:10.1016/j.euromechflu.2007.10.005.

Racina, A. and Kind, M., Specific power input and local micromixing times in turbulent Taylor-Couette flow, Experiments in Fluids, Vol. 41, pp. 513–522, (2006), DOI:10.1007/s00348-006-0178-x.

Reynolds, O., On the extent and action of the heating surface of steam boilers, Papers on Mechanical and Physical subjects, p. 81, (1901).

Takeda, Y., Quasi-periodic state and transition to turbulence in a rotating Couette system, Journal of Fluid Mechanics, Vol. 389, pp. 81–99 (1999), DOI:10.1017/S0022112099005091.

Taylor, G. I., VIII. Stability of a viscous liquid contained between two rotating cylinders, Philosophical Transactions of the Royal Society A, Vol. 223, 289 LP–343 (1923), DOI:10.1098/rsta.1923.0008.

Teng, H., Liu, N., Lu, X., and Khomami, B. Direct numerical simulation of Taylor-Couette flow subjected to a radial temperature gradient, Physics of Fluids, Vol. 27, 125101 (2015), DOI:10.1063/1.4935700.

Uchino, K., Mamori, H., and Fukagata, K., Heat transfer in fully developed turbulent channel flow with streamwise traveling wave-like wall deformation, Journal Thermal Science and Technology, Vol. 12, 16-00624 (2017), DOI:10.1299/jtst.2017jtst0003.

Wang, L., Olsen, M.G., and Vigil, R.D., Reappearance of azimuthal waves in turbulent Taylor–Couette flow at large aspect ratio, Chemical Engineering Science, Vol. 60, pp. 5555–5568 (2005), DOI:10.1016/j.ces.2005.05.024.

Yamamoto, A., Hasegawa, Y., and Kasagi, N., Optimal control of dissimilar heat and momentum transfer in a fully developed turbulent channel flow, Journal of Fluid Mechanics, Vol. 733, pp. 189–220 (2013), DOI:10.1017/jfm.2013.436.